JBC Papers in Press. Published on January 5, 2012 as Manuscript M111.316075
The latest version is at http://www.jbc.org/cgi/doi/10.1074/jbc.M111.316075

Structural insights into apoptotic DNA degradation by CED-3 Protease Suppressor-6 (CPS-6) from *Caenorhabditis elegans**

Jason L. J. Lin[1], Akihisa Nakagawa[2], Chia Liang Lin[1,3], Yu-Yuan Hsiao[1], Wei-Zen Yang[1], Yi-Ting Wang[1], Lyudmila G. Doudeva[1], Riley Robert Skeen-Gaar[2], Ding Xue[2] and Hanna S. Yuan[1,4*]

[1]From the Institute of Molecular Biology, Academia Sinica, Taiwan, ROC.
[2]Department of Molecular, Cellular and Developmental Biology, University of Colorado, Boulder, Colorado, USA.
[3]Institute of Bioinformatics and Structural Biology, National Tsing Hua University, Taiwan, ROC.
[4]Graduate Institute of Biochemistry and Molecular Biology, National Taiwan University, Taiwan, ROC.

*Running title: *Crystal structure of CPS-6*

To whom correspondence should be addressed: Hanna S. Yuan, Institute of Molecular Biology, Academia Sinica, Taipei, Taiwan 11529, Tel: 886-2-27884151; Fax: 886-2-27826085; E-mail: hanna@sinica.edu.tw

Keywords: crystal structure, Endonuclease G, chromosome fragmentation, DNase, nuclease, protein-DNA interactions.

Background: CPS-6 (EndoG) degrades chromosomal DNA during apoptosis.
Results: Crystal structure of *C. elegans* CPS-6 was determined, and the DNA binding and cleavage mechanisms by CPS-6 were revealed.
Conclusion: The DNase activity of CPS-6 is positively correlated with its pro-cell death activity.
Significance: This study improves our general understanding of DNA hydrolysis by ββα-metal finger nucleases and the process of apoptotic DNA fragmentation.

SUMMARY

Endonuclease G (EndoG) is a mitochondrial protein that traverses to the nucleus and participates in chromosomal DNA degradation during apoptosis in yeast, worms, flies and mammals. However, it remains unclear how EndoG binds and digests DNA. Here we show that the *C. elegans* CPS-6, a homologue of EndoG, is a homodimeric Mg^{2+}-dependent nuclease, binding preferentially to G-tract DNA in the optimum low-salt buffer at pH 7. The crystal structure of CPS-6 was determined at 1.8 Å resolution, revealing a mixed αβ topology with the two ββα-metal finger nuclease motifs located distantly at the two sides of the dimeric enzyme. A structural model of the CPS-6-DNA complex suggested a positively charged DNA-binding groove near the Mg^{2+}-bound active site. Mutations of four aromatic and basic residues, F122, R146, R156 and F166, in the protein-DNA interface significantly reduced the DNA binding and cleavage activity of CPS-6, confirming that these residues are critical for CPS-6-DNA interactions. In vivo transformation rescue experiments further showed that the reduced DNase activity of CPS-6 mutants was positively correlated with its diminished cell killing activity in *C. elegans*. Taken together, these biochemical, structural, mutagenesis and in vivo data reveal a molecular basis of how CPS-6 binds and hydrolyzes DNA to promote cell death.

EndoG was first identified as a mitochondrial DNase that prefers to cleave phosphordiester bonds of DNA at $(dG)_n$ tracts in yeasts and mammals (1-3). It was later recognized as one of the apoptotic nucleases that participate in chromosome

fragmentation during apoptosis in mice and worms (4,5). Apoptotic nucleases have attracted attention because their inactivation may produce undigested DNA that lead to autoimmune disorders, including systemic lupus erythematosus and rheumatoid arthritis (6,7). In the search of apoptotic nucleases, CAD/DFF40 was the first one identified in mammals (8,9). EndoG was subsequently discovered as an apoptotic DNase released from mitochondria, mediating residual DNA fragmentation in CAD/DFF40-decificient mice (5). An independent genetic screen for cell-death effectors also identified CPS-6, an EndoG homolog, to be a nuclease important for apoptotic chromosome fragmentation in *C. elegans* (4). CPS-6 in *C. elegans* and EndoG in mouse and yeast were shown to be compartmented in the mitochondrial intermembrane space so that it does not affect nuclear genomic DNA in non-apoptotic cells; in response to apoptotic signals, it is released and translocated to the nucleus to digest chromosomal DNA (10).

Biochemical and genetic evidence further showed that *C. elegans* CPS-6 associates and cooperates with WAH-1, a *C. elegans* homolog of apoptosis-inducing factor (AIF), and CRN-1 (cell death related nucleases) to promote DNA degradation during apoptosis (11,12). Mammalian EndoG also interacts with AIF and FEN-1 (a CRN-1 homolog) (13). Therefore the roles of CPS-6 and EndoG in apoptotic chromosome fragmentation are likely conserved. Indeed, mouse EndoG can rescue the cell death defects of the *cps-6* mutant in *C. elegans* (4). Apart from CPS-6, a number of nucleases have been identified that are involved in chromosome fragmentation during apoptosis in *C. elegans*, including NUC-1, DCR-1 and cell death-related nucleases (CRN-1 to 7)(14-17). CPS-6 interacts not only with CRN-1 and WAH-1 but also with CRN-3, CRN-4, CRN-5 and CYP-13, and these proteins, likely in the form of a multi-nuclease complex, work together to promote apoptotic DNA fragmentation (14). Inactivation of *cps-6* (the gene encoding CPS-6) resulted in the accumulation of TUNEL-positive cells and delayed appearance of embryonic cell corpses during development, suggesting that CPS-6 is required for normal apoptotic DNA degradation (14). Knockout of the EndoG gene in mice did not cause significant phenotypes either in embryogenesis or in apoptosis, possibly due to the presence of redundant apoptotic nucleases and various apoptotic DNA degradation pathways during apoptosis (18,19).

Investigation of the cellular functions of EndoG suggests that this nuclease not only has a pro-death role in apoptosis but also plays a pro-life role in mitochondrial DNA replication and recombination (20,21). The conflicting life vs death role of EndoG was clarified in budding yeast in which EndoG functions as a potent cell-death inducer only under high respiration conditions in a caspase- and AIF-independent mechanism, while EndoG promotes cell viability under high cell-division conditions (22). Thus yeast EndoG can act either as a crucial but uncharacterized molecule in mitochondria for cell proliferation, or be switched to a death executioner, digesting chromosomal DNA in the nucleus during apoptosis in a caspase-independent pathway.

Mammalian, *Drosophila*, *C. elegans* and yeast CPS-6/EndoG share sequence homology with *Serratia* nuclease, which contains a conserved DRGH sequence in the ββα-metal finger motif that has been identified in a number of other bacterial nonspecific nucleases (see Figure 1) (23,24). Yeast and mammalian EndoG are Mg^{2+}-dependent homodimeric proteins with a preference for single-stranded RNA and DNA substrates (3). *Drosophila* EndoG particularly has a nuclear inhibitor EndoGI which likely protects the cell against low levels of EndoG that leaks out from mitochondria (25). The crystal structure of *Drosophila* EndoG in complex with its inhibitor EndoGI has been reported, revealing how the monomeric EndoGI inhibits the activity of the dimeric EndoG by blocking its active site and oligonucleotide-binding groove (26).

Although the pro-death role of CPS-6/EndoG has been studied most extensively in *C. elegans*, the biochemical and structural information for CPS-6 remains unknown. To understand the intriguing life vs death role of CPS-6, we employed a range of biochemical assays in combination with X-ray

crystallography to determine the crystal structure of CPS-6 bound with a Mg^{2+} cofactor in the active site at a high resolution of 1.8 Å. This structural information led to the identification of the critical DNA binding residues, which were verified through site-directed mutagenesis and several different in vitro assays, and provided invaluable insights for in vivo functional assays. In particular, reduced DNase activities of the CPS-6 mutants positively correlated with their decreased pro-apoptotic activities in *C. elegans*. This study thus provides a molecular basis for the DNA binding and hydrolysis by CPS-6 during apoptosis.

EXPERIMENTAL PROCEDURES

Cloning, protein expression, and purification- The genes encoding CPS-6 (CPS-6 residues 63-305) and WAH-1 (WAH-1 residues 214-700) were amplified by PCR, using Taq DNA polymerase (Stratagene). The primers used for CPS-6 PCR were 5'-GATGCAGGATCCCCATCTCGTTCGGCA-3' (forward) and 5'-CAATCAAAGCTTTCATCCTCCCTTCTTTGC-3' (reverse). The primers used for cAIF PCR were 5'-GCGGGATCCTCCGAACAACAATCGATGAA GCC-3' (forward) and 5'-GCGCTGCAGCTAAGCACTCTTCGCATC-3' (reverse). The PCR-amplified genes were cloned into the BamHI/HindIII or BamHI/PstI site, respectively, of the expression vector pQE30 (Qiagen) to generate the His-tagged fusion constructs. All CPS-6 point mutants were generated using the QuickChange site-directed mutagenesis kits (Stratagene).

Single colonies of the *E. coli* strain M15 transformed with pQE30-CPS-6-(63-305) or pQE30-WAH-1-(214-700) plasmids were inoculated into 10 ml of LB medium supplemented with 100 μg/ml ampicillin, and grown at 37°C overnight. The overnight cultures were grown to an OD_{600} of 0.6 and then induced with 0.8 mM IPTG at 18°C for 20 h. The harvested cells were disrupted by a microfluidizer in a buffer containing 50 mM HEPES (pH 7.4), 300 mM NaCl, 10 mM imidazole and 5% glycerol. The crude cell extract was passed through a TALON® metal affinity resin column (BD Biosciences) followed by a gel filtration chromatography column (Superdex 200, GE Healthcare) in 50 mM Tris-HCl (pH 7.4), 500 mM NaCl, and 2.5 mM DTT. Purified protein samples were concentrated to suitable concentrations and stored at -80°C until use.

Nuclease activity assays- For the DNase activity assays shown in Figure 2C, a PCR-amplified 1.6 kb linear double-stranded DNA fragment (40 ng) was incubated with purified protein (0-0.1 μM) in a buffer containing 50 mM MES (pH 6.0), 25 mM NaCl, 5 mM $MgCl_2$, and 1 mM DTT. To investigate pH effects on the DNase activity, as shown in Figure 2D, pET28 plasmid DNA (25 ng) was incubated with 2 μM purified protein in 100 mM NaCl, 2 mM $MgCl_2$, 2 mM DTT and various buffers of 10 mM of sodium acetate trihydrate (pH 4), tri-sodium citrate dehydrate (pH 5), sodium cacodylate (pH 6), sodium HEPES (pH 7), Tris-HCl (pH 8), CAPSO (pH 9) and CAPS (pH 10 and 11). For examine salt effects on the DNase activity, as shown in Figure 2E, pET28 plasmid DNA (25 ng) was incubated with 2 μM purified protein in a reaction buffer containing 10 mM HEPES (pH 7.0), 2 mM $MgCl_2$, 2 mM DTT, and various concentrations of NaCl (25 to 500 mM). For the DNase activity assays shown in Figure 3A, purified wild-type CPS-6 (0.03 to 2 μM) was incubated with pET28 plasmid DNA (25 ng) in the optimal CPS-6 buffer (10 mM HEPES (pH 7.0), 100 mM NaCl, 2 mM $MgCl_2$, and 2 mM DTT). For the DNase activity assays shown in Figure 3B, purified wild-type CPS-6 (0.06 to 2 μM) was incubated with 60 nM 48-mer ssDNA (5'-ACGCTGCCGAATTCTGGCGTTAGGAGATA CCGATAAGCTTCGGCTTAA) or dsDNA (above 48-mer ssDNA annealed with its complementary sequence), both of which were ^{32}P-labeled at the 5'-end in the optimal CPS-6 buffer. For the DNase activity assays shown in Figure 3C, purified wild-type protein (0.25 to 1 μM) was incubated with either 10 nM 11-mer ssDNA (5'-AACCTTACAAC-3') or ssRNA (5'-AACCUUACAAC-3'), both of which were labeled at the 5'-end with ^{32}P, in the optimal CPS-6 buffer. For the DNase activity assays shown in Figure 5C, purified wild-type and mutated CPS-6 (2

μM) were incubated with pET28 plasmid DNA (25 ng) in the optimal CPS-6 buffer. All reactions were incubated at 37°C for 1 h. The digested DNA samples were resolved on a 1% agarose gel (Figures 2C-2E and 3A), stained by ethidium bromide, and detected with a charge-coupled device camera at UV trans-illumination. In Figure 3B, the digested DNA samples were resolved in a 20% native polyacrylamide gel and run in 1x TBE (90 mM Tris-Borate, 2.0 mM EDTA). In Figure 3C, the digested DNA or RNA samples were resolved in a 20% denaturing polyacrylamide gel (8 M urea) run in 1x TBE (90 mM Tris-Borate, 2.0 mM EDTA). The gel was subsequently exposed to a phosphorimaging plate (Fujifilm) and visualized using an FLA-5000 (Fujifilm) imaging system.

Filter binding assay- Single-stranded DNA substrates for the filter binding assay were 5'-end labeled with [γ-^{32}P]ATP by T4 polynucleotide kinase. The ^{32}P-labeled DNA (14 fmol) were incubated with the serial dilution of protein samples in the binding buffer containing 10 mM HEPES, pH 7.0, 100 mM NaCl, 2 mM DTT and 2 mM EDTA for 30 min at room temperature. The reaction mixtures were then passed through the filter binding assay apparatus (Bio-Dot SF microfiltration apparatus, Bio-Rad). After extensive washing, the CPS-6-DNA complex-bound nitrocellulose membrane and free DNA-bound nylon membrane were air dried and exposed to a phosphorimaging plate. The intensities of CPS-6-DNA complex and free DNA were quantified by the program AlphaImager IS-2200 (Alpha Innotech, USA). The binding percentages were calculated and normalized. The apparent K_d values were estimated by one-site binding curve fitting using GraphPad Prism 4.

Immunoprecipitation-His-tagged CPS-6 (22-308) H148A mutant (1 μg) was mixed with 1 μg His-tagged WAH-1 (214-700) and incubated for 2 h at 4^{o}C in buffer containing 50 mM Tris-HCl (pH 7.0), 300 mM NaCl, 10% glycerol and 5 mM DTT. This reaction was followed by the addition of anti-CPS-6 (polyclonal rabbit; 1:100 dilution) and continued to be agitated at 4^{o}C for 2 h. Protein G beads (Amersham Biosciences) were then added to the reaction mixture, followed by incubation for 2 h at 4^{o}C. The protein beads were then centrifuged and the supernatant was removed. After washing three times with reaction buffer, the beads were loaded onto a 10% SDS-PAGE followed by the detection of immunoblotting using anti-His antibodies (monoclonal mouse).

In vivo cell death assay- $P_{dpy\text{-}30}$CPS-6 construct was used for in vivo expression (4). To construct $P_{dpy\text{-}30}$CPS-6(H148A), $P_{dpy\text{-}30}$CPS-6(R146A), and $P_{dpy\text{-}30}$CPS-6(F166A), Hind III-Pst I fragments, including the corresponding mutations, were excised from pQE30-CPS-6(H148A), pQE30-CPS-6(R146A), and pQE30-CPS-6(F166A), respectively, and subcloned into the $P_{dpy\text{-}30}$CPS-6 construct by replacing the wild-type fragment via its HindIII and PstI sites.

C. elegans strains were maintained using standard procedures (27). The CPS-6 expression constructs (at 20 μg/ml) were injected into *cps-6(sm116)* animals as previously described (28), using the pTG96 plasmid (at 20 μg/ml) as a co-injection marker, which directs GFP expression in all cells in most developmental stages (29). The numbers of cell corpses in living GFP-positive transgenic embryos were determined using Nomarski optics as described previously (30).

Crystallization and crystal structural determination- Crystals of CPS-6 were grown by the hanging-drop vapor diffusion method at 4^{o}C. The crystallization drop was made by mixing 0.5 μl of protein solution and 0.5 μl of reservoir solution. The CPS-6 H148A mutant (10 mg/ml in 50 mM Tris-HCl (pH 7.4), 500 mM NaCl and 2.5 mM DTT) was crystallized using a reservoir solution containing 6% Tacsimate, 0.1 M MES (pH 6.0) and 25% PEG4000. Diffraction data were collected at the BL44XU beamline at SPring-8, Japan, and were processed and scaled by HKL2000. The crystal structure was solved by the molecular replacement method using the crystal structure of *Drosophila melanogaster* EndoG (PDB ID: 3ISM, chains A and B) as the search model by program MOLREP of CCP4. The models were modified by Coot and refined by Phenix. The diffraction and refinement statistics are listed in Table 1. Structural coordinates and diffraction structure factors have been deposited in the RCSB Protein Data Bank with

the PDB ID code of 3S5B for CPS-6 H148A mutant.

RESULTS

Recombinant CPS-6 is a functional homodimeric endonuclease- To investigate the structure and biochemical properties of CPS-6, the recombinant wild-type 6xHistidine-tagged CPS-6 (residues 63-305) was expressed in *E. coli*. The N-terminal residues (1-62) and the C-terminal residues (306-308) were not included for expression. However, the expression level of the wild-type CPS-6 was low due to its toxic DNase activity in *E. coli*. Therefore the putative general base residue H148 was mutated to generate a CPS-6 mutant (H148A), which can be expressed in a large amount. The N-terminal sequence (residues 1 to 62) was removed because it was unstable and degraded with time. The wild-type and mutated CPS-6 (residues 63-305) proteins were expressed and purified by chromatographic methods using a Ni^{2+}-NTA affinity column, followed by a Superdex 200 gel filtration column. They were purified to homogeneity as confirmed by SDS-PAGE (Figure 2A). The recombinant CPS-6 appeared as a dimeric protein as determined by size-exclusion chromatography on a Superdex 200 column (Figure 2B), with an apparent native molecular weight of about 48 kD (calculated molecular weight of CPS-6 monomer: 28.5 kD).

The nuclease activity of purified wild-type CPS-6 was analyzed by incubation of CPS-6 with a linear 1.6-kb DNA fragment in a buffer containing 25 mM NaCl and 5 mM $MgCl_2$ for one hour. A relatively rapid degradation of DNA was observed with wild-type CPS-6, but not with the H148A mutant, as a function of increasing protein concentration (Figure 2C). Furthermore, CPS-6 (0 to 1 μM) was incubated with DNA in the presence and absence of EDTA. CPS-6 had significantly reduced DNase activity in the presence of EDTA, suggesting that divalent metal ions are required for the enzyme activity of CPS-6 (supplemental Figure S1). The optimal conditions for the nuclease activity of CPS-6 were further characterized over a wide range of pH values and salt concentrations. CPS-6 digested plasmid DNA most efficiently at neutral pH and at low salt concentrations (25-100 mM NaCl) in the presence of 2 mM $MgCl_2$ (Figure 2D, E). A relatively more efficient nuclease activity for CPS-6 was found at pH values ranged from 7 to 10 than that of 4 to 6 in the presence of 100 mM NaCl (Figure 2D). Given the pKa value of ~6 for His148, acidic conditions might have caused its protonation and hence the loss of the general base function. Moreover, high-salt buffers might interfere with the interactions between the positively charged CPS-6 and negatively charged DNA.

The recombinant CPS-6(H148A) mutant was further tested for its ability to interact with WAH-1 by immunoprecipitation. Anti-CPS-6 antibody was used to pull down the CPS-6/WAH-1 complex, which was detected by western blotting using anti-His antibodies. This experiment showed that the purified recombinant His-tagged CPS-6 interacted directly with the purified His-tagged WAH-1 (see Figure 2F). Taken together, these results show that the recombinant CPS-6 was a fully functional protein, capable not only of DNA digestion but also of interaction with WAH-1.

CPS-6 digests RNA and DNA with a preference for binding a G-track DNA- To determine the substrate preference for CPS-6, pET28 plasmid DNA (25 ng) was used as the substrate in a concentration-course experiment under the reaction conditions of 100 mM NaCl and 2 mM $MgCl_2$ at pH 7. CPS-6 cleaved plasmid DNA in a concentration-dependent manner, steadily converting the supercoiled DNA into the open-circular and linear forms, when the concentration of CPS-6 was increased from 0.03 to 2 μM (Figure 3A). Significant amount of DNA digestion, visible as a broad smear, was observed when the protein concentration was increased to 2 μM (Figure 3A). This result confirms that CPS-6 has endonuclease activity.

Linear ssDNA and dsDNA substrates (48-mers) were next used for digestion experiments with wild-type CPS-6 (residues 63-305). We observed that ssDNA was cleaved a bit more efficiently than dsDNA (Figure 3B). A comparison between 11-mer ssDNA and ssRNA showed that wild-type CPS-6 (residues 63-305) digested 11-mer ssRNA more efficiently than 11-mer ssDNA (Figure 3C). These results show that CPS-6 digests both DNA and RNA

and prefers single-stranded nucleic acid substrates slightly over double-stranded ones, in agreement with earlier findings with yeast and mammalian EndoG (3).

To investigate the sequence preference for CPS-6, four 5'-end-^{32}P-labeled 14-nucleotide single-stranded DNA containing 0, 2, 4 and 6 consecutive G nucleotides were used for protein-DNA binding experiments (Figure 3D). The inactive CPS-6 mutant H148A was used for the protein-DNA binding assays to avoid DNA digestion by CPS-6. The dissociation constants measured between CPS-6(H148A) and DNA were increased hierarchically from $(dG)_6$, $(dG)_4$, $(dG)_2$ to $(dG)_0$ DNA (Kd: 0.53±0.02 μM for $(dG)_6$, 1.13±0.73 μM for $(dG)_4$, 2.55±0.21 μM for $(dG)_2$, 5.14±0.36 μM for $(dG)_0$). Hence, this result shows that CPS-6 prefers to bind DNA with G-tract sequences.

Crystal structure of the dimeric CPS-6 reveals a basic DNA-binding groove- To determine the crystal structure of CPS-6, the H148A mutant was used for crystallization screening experiments because the inactive H148A mutant can be expressed and purified in a larger quantity as compared to wild-type CPS-6. The H148A CPS-6 mutant was crystallized by the hanging drop vapor diffusion method. X-ray diffraction data up to a resolution of 1.8 Å were collected. CPS-6 H148A mutant was crystallized in the space group $P2_1$ with one dimer per asymmetric unit. The crystal structure of CPS-6 (residues 63-305, H148A mutant) was determined by molecular replacement using the *Drosophila melanogaster* EndoG structure (PDB entry: 3ISM) as the search model. The crystal structure was refined to an R-factor of 16.6% for 41,201 reflections and an R-free of 21.0 % for 1,876 reflections from 37.6 to 1.8 Å (Table 1).

CPS-6 has a mixed αβ topology similar to that of *Serratia* nuclease (31) and EndA (32) with a central six-stranded β-sheet packed against the rest of the α-helices and β-strands (see Figure 4). The two ββα-metal finger motifs (shown in cyan), consisting of the conserved ^{145}DRGH^{148} sequence in one of the β-strands, are located distantly on the two sides of the homodimer. A long β-strand (β8) from each protomer forms an antiparallel β-sheet at the dimeric interface. The two protomers are well packed with sufficient buried interfaces of 1392.2 Å^2 to stabilize the dimeric structure.

Although magnesium ions were not present in the crystallization buffer, a Mg^{2+} was bound to Asn180 in the ββα-metal finger motif in the crystal structure of CPS-6. The omit map clearly shows that Mg^{2+} coordinated to Asn180 and five water molecules in an octahedral geometry (Figure 4B). The conformation of the active site of CPS-6 is similar to other nucleases containing a ββα-metal finger motif in which His148 in the conserved ^{145}DRGH^{148} sequence functions as a general base to activate a water molecule, and the Mg^{2+}-bound water molecule likely functions as a general acid to provide a proton for the 3'-phosphate leaving group (24). Moreover, the amide side chain of the metal-binding residue Asn180 formed a hydrogen bond (2.69 Å) with the carboxylate side chain of Asp145, showing that Asp145 in the conserved ^{145}DRGH^{148} sequence is important for stabilizing the metal ion-binding residue in the CPS-6 active site. On the other hand, Arg146 within the conserved ^{145}DRGH^{148} sequence is likely involved in DNA binding (see the mutagenesis results in the next section).

The electrostatic potential mapping onto the CPS-6 structure further shows a basic groove extending on the molecule next to the active site (see Figure 4C). It has been shown that endonucleases containing a ββα-metal finger motif, such as I-PpoI, Vvn and ColE7, bind to DNA in a similar mode, i.e., the relative orientations between the ββα-metal finger motif and DNA are comparable (33). A model of the CPS-6-DNA complex was thus constructed by superimposition of the ββα-metal motif of CPS-6 (residues 144-155 and 170-182) with that of Vvn (residues 77-82 and 118-129) in the Vvn-DNA complex (PDB code: 1OUP). After removal of Vvn, the DNA was well fitted onto the surface of CPS-6 with one phosphate backbone bound to the basic groove around the active site (see Figure 4C). We therefore suggest that the phosphate backbone of DNA is likely bound and digested at this basic groove in CPS-6.

Critical DNA-binding residues in CPS-6- The

CPS-6-DNA complex model suggests that DNA binds to a site located in proximity to the active site in the dimeric CPS-6 (Figure 5A). A closer look at the model revealed five amino acid residues located near DNA: the two aromatic residues Phe122 and Phe166, and the three basic residues Arg117, Arg146 and Arg156 (Figure 5B). In order to investigate the influence of these residues on the nuclease activity of CPS-6, site-directed mutagenesis was employed to selectively mutate those amino acid residues located within the interfacial region of the CPS-6-DNA complex model. We found that the nuclease activity of four mutant proteins, except R117A, was reduced significantly, with F122A, R156A and F166A digesting the least amount of DNA, and R146A digesting less amount of DNA as compared to that of wild-type CPS-6 (Figure 5D).

To determine if these residues were involved in DNA binding, double mutants H148A/R117A, H148A/F122A, H148A/R146A, H148A/R156A and H148A/F166A were constructed and purified to obtain inactive mutants that cannot digest DNA substrates (supplemental Figure S2). Filter binding assays were employed to determine the dissociation constants between CPS-6 double mutants and single-stranded 48-nt DNA substrates. The dissociation constants had the same trend as those of activity assays (see Figure 5D and 5E). H148A and H148A/R117A had highest affinity for DNA with a Kd of 245±18 nM and 249±20 nM, respectively. This result suggests that R117 was not involved in DNA binding and therefore R117A had retained DNase activity. Conversely, the Kd values for other mutants with low DNase activities were increased significantly (707±88 nM for H148A/F122A, 468±42 for H148A/R146A, 652±111 nM for H148A/R156A and 658±74 nM for H148A/F166A). These results confirm our model suggesting that Phe122, Arg146, Arg156 and Phe166 are important amino acid residues that are involved in DNA binding and digestion in CPS-6.

Residues at the CPS-6 catalytic site or involved in DNA binding are important for apoptosis-promoting activity in C. elegans- To examine whether critical residues identified by structural predictions and in vitro nuclease assays are important for *cps-6* cell killing activity in vivo, full-length CPS-6 or CPS-6 mutants was expressed in the *cps-6* deficient strain *(sm116)* under the control of the *dpy-30* gene promoter ($P_{dpy\text{-}30}$CPS-6), which directs ubiquitous gene expression in *C. elegans* (34). Compared with wild-type animals, the *cps-6(sm116)* mutant displayed a delay-of-cell-death defect during embryonic development (4): less cell corpses were observed at early embryonic stages (comma and 1.5-fold stages) and more cell corpses were seen at later embryonic stages (2-fold, 2.5-fold, and 3-fold stages)(Figure 6A). Expression of wild-type CPS-6 fully rescued the delay-of-cell-death defect of the *cps-6(sm116)* mutant (Figure 6A). In contrast, expression of CPS-6 harboring a catalytic site mutation (H148A) failed to rescue the cell death defect of *cps-6(sm116)* animals (Figure 6B). Interestingly, expression of either CPS-6(R146A) or CPS-6(F166A), both of which showed significantly reduced nuclease activity (Figure 5D), partially rescued the *cps-6(sm116)* mutant (Figure 6C and 6D). These results indicate that the DNA binding residues and the catalytic site of CPS-6 are important for its nuclease activity *in vitro* and pro-apoptotic activity *in vivo*.

DISCUSSION

Catalytic mechanism of CPS-6 in DNA hydrolysis-In this study, we used CPS-6 as a model system for biochemical and structural analysis. CPS-6 shares a high sequence identity of 50%, 49%, 55% and 39% with human, bovine, fruit fly and yeast EndoG, respectively (Figure 1). We determined the high-resolution crystal structure of CPS-6 and revealed that the highly conserved ^{145}DRGH^{148} sequence is located within the ββα-metal finger motif. The geometry of the active site of CPS-6 is similar to the ones observed in other ββα-metal finger nucleases, all of which display a divalent metal ion bound to 1 or 2 amino acid residues and four or five water molecules, including I-PpoI (35), Hpy99I (36), T4 EndoVII (37), I-HmuI (38), *Serratia* nuclease (31), EndA (32), NucA (39) and Vvn (40).

The comparison of the active site between CPS-6 and Vvn shows clearly that several catalytic residues

are located at similar positions, including the general base residue His148 (mutated to Ala) in CPS-6 and His80 in Vvn, and the metal-binding residue Asn180 in CPS-6 and Asn127 in Vvn (see Figure 7A). The mutation of His148 to Ala abolished the enzyme activity of CPS-6 (Figure 2C), supporting the role of His148 as the general base residue. The general base residue His80 in Vvn is polarized by a hydrogen bond to the carbonyl group of Glu113, where similarly the general base residue His148 in CPS-6 can be polarized by a hydrogen bond to the carbonyl group of Thr165. The metal ion-bound residue Asn127 in Vvn is fixed by a hydrogen bond network to the side chain of Glu77 and Arg72, where similarly, Asn180 in CPS-6 makes a hydrogen bond network to Asp145 and Arg181. In summary, these two non-specific ββα-metal finger nucleases share similar active site architectures.

A parallel hydrolysis mechanism analogous to that of Vvn is therefore proposed for CPS-6, with His148 functioning as a general base to activate a water molecule for the in-line attack on the scissile phosphate, and a Mg^{2+}-bound water molecule functioning as a general acid to provide a proton to the 3'-oxygen leaving group (see Figure 7B). Structural modeling of the CPS-6-DNA complex further reveals a basic DNA-binding groove constituted by basic residues Arg146, and Arg156, and nearby aromatic residues Phe122 and Phe166 (Figure 5B). Site-directed mutagenesis confirmed that these basic and hydrophobic residues (Arg146, Arg156, Phe122 and Phe166) are critical for DNA-binding and cleavage activity of CPS-6 (Figure 5C and 5D). Arginine residues are frequently located within protein-DNA interfaces, and preferentially make hydrogen bonds to guanine (41). On the other hand, phenylalanine side chains often stack with DNA bases, with a preference for thymine, adenine and cytosine, but not guanine (41,42). It is speculated that the preference of EndoG for the cleavage of poly-(dG) tracks in DNA is linked in part to these basic and phenylalanine residues, particularly the preference of arginine residues for making hydrogen bonds with guanine bases.

Given the obvious impacts of these CPS-6 mutations on the nuclease activity of CPS-6 and CPS-6 DNA binding affinity (Figure 5), it is of interest in this study to address the functional role of those mutants in vivo. An identical delay-of-cell-death defect was observed in the catalytic-site CPS-6 mutant (H148A) (lacking the DNase activity) to that of the *cps-6* deficient animal, *cps-6(sm116)* (Figure 6B). In contrast, expression of the CPS-6 DNA-binding-site mutants (R146A and F166A) that still have residual DNase activity can partially rescue the cell death defect of the *cps-6(sm116)* mutant (Figures 6 C and D). Therefore, the reduced nuclease activity of CPS-6 is positively correlated to its diminished cell killing activity in *C. elegans*.

Different dimeric interfaces of CPS-6- The crystal structure of CPS-6 reveals an overall mixed αβ topology similar to that of *Serratia* nuclease (31) with a ββα-metal finger motif situated on one face of the central β-sheet. Apart from *Serratia* nuclease, a number of other ββα-metal finger nucleases are also homodimeric enzymes, including I-PpoI, Hpy99I and T4 Endo VII. I-PpoI is a homing endonuclease that generate staggered products with four-nucleotide 3' overhangs (43), whereas Hpy99I is a restriction endonuclease that generates staggered products with five-nucleotide 3' overhangs (36). The reported crystal structures of I-PpoI-DNA and Hpy99I-DNA complexes show that the two ββα-metal finger motifs are orientated in a similar way, with close distances of 15.1 Å and 20.4 Å between the two Mg^{2+} ions in I-PpoI and Hpy99I, respectively (see Figure 8B). Moreover, the two ββα-metal finger motifs are located closely to the DNA sugar-phosphate backbones so that each monomer can make one nick on one strand of the double-stranded DNA to produce precisely the staggered-end products. On the other hand, the two ββα-metal finger motifs in the Holliday junction resolvase T4 Endo VII are arranged more distantly (26.1 Å between the two Mg^{2+} ions) in a different relative orientation for the binding and cleavage of a four-way DNA junction (44). Interestingly, in these three protein-DNA complexes, the 2-fold symmetry axis between the two protomers roughly coincides with the 2-fold axis of the DNA substrates (see the 2-fold axis marked in Figure 8B). Therefore, the

relative orientation and distance of the two ββα-metal finger motifs in these dimeric endonucleases is actually restrained by their substrates.

On the other hand, CPS-6 is a non-specific endonuclease, and it shares not only a similar fold but also a similar activity to that of *Serratia* nuclease. However, CPS-6 dimerizes in a way completely different from that of *Serratia* nuclease. Superimposition of one of the protomers of the dimeric structure of CPS-6 and *Serratia* nuclease shows that the dimeric interfaces are located in different regions in the two proteins (see Figure 8A). As a result, the relative orientation and distances between the two ββα-metal finger motifs are different in the two non-specific endonucleases, 44.5 Å in CPS-6 and 54.4 Å in *Serratia* nuclease for the distance between the two Mg^{2+} ions. This result indicates that each monomer of CPS-6 and *Serratia* nuclease likely interacts with DNA substrates independently. Hence, the relative orientation of the two distant ββα-metal finger motifs in these non-specific nucleases is irrelevant. Why CPS-6 and *Serratia* nuclease did not evolve into monomeric enzymes, such as the non-specific nucleases EndA, NucA and Vvn, is unknown. In the future, it will be necessary to co-crystallize CPS-6 with DNA to further elucidate its substrate binding mode and the basis of sequence preference.

REFERENCES

1. Ruiz-Carrillo, A., and Renaud, J. (1987) *EMBO J.* **6**, 401-407
2. Cummings, O. W., King, T. C., Holden, J. A., and Low, R. L. (1987) *J. Biol. Chem.* **262**, 2005-2015
3. Low, R. L. (2003) *Mitochondrion* **2**, 225-236
4. Parrish, J., Li, L., Klotz, K., Ledwich, D., Wang, X., and Xue, D. (2001) *Nature* **412**, 90-94
5. Li, L. Y., Luo, X., and Wang, X. (2001) *Nature* **412**, 95-99
6. Napirei, M., Karsunky, H., Zevnik, B., Stephan, H., Mannherz, H. G., and Möröy, T. (2000) *Nature Genet.* **25**, 177-181
7. Kawane, K., Ohtani, M., Miwa, K., Kizawa, T., Kanbara, Y., Yoshioka, Y., Yoshikawa, H., and Nagata, S. (2006) *Nature* **443**, 998-1002
8. Liu, X., Zou, H., Slaoghter, C., and Wang, X. (1997) *Cell* **89**, 175-184
9. Enari, M., Sakahira, H., Yokoyama, H., Okawa, K., Iwamatsu, A., and Nagata, S. (1998) *Nature* **391**, 42-50
10. Widlak, P., and Garrard, W. T. (2005) *J. Cell. Biochem.* **94**, 1078-1087
11. Wang, X., Yang, C., Chai, J., Shi, Y., and Xue, D. (2002) *Science* **298**, 1587-1592
12. Parrish, J. Z., Yang, C., Shen, B., and Xue, D. (2003) *EMBO J.* **22**, 3451-3460
13. Kalinowska, M., Garncarz, W., Pietrowska, M., Garrard, W. T., and Widlak, P. (2005) *Apoptosis* **10**, 821-830
14. Parrish, J. Z., and Xue, D. (2003) *Molecular cell* **11**, 987-996
15. Wu, Y.-C., Stanfield, G. M., and Horvitz, H. R. (2000) *Genes & Develop.* **14**, 536-548
16. Nakagawa, A., Shi, Y., Kage-Nakadai, E., Mitani, S., and Xue, D. (2010) *Science* **328**, 327-334
17. Lai, H.-J., Lo, S. J., Kage-Nakadai, E., Mitani, S., and Xue, D. (2009) *Plos One* **10**, e7348
18. Irvine, R. A., Adachi, N., Shibata, D. K., Cassell, G. D., Yu, K., Karanjawala, Z. E., Hsieh, C.-L., and Lieber, M. R. (2005) *Mol. Cell. Biol.* **25**, 294-302
19. David, K. K., Sasaki, M., Yu, S.-W., Dawson, T. M., and Dawson, V. L. (2006) *Cell Death Differ.* **13**, 1147-1155
20. Cote, J., and Ruiz-Carrillo, A. (1993) *Science* **261**, 765-769
21. Huang, K.-J., Ku, C.-C., and Lehman, I. R. (2006) *Proceedings of the National Academy of Sciences of the United States of America* **103**, 8995-9000
22. Buttner, S., Eisenberg, T., Carmona-Gutierrez, D., Ruli, D., Knauer, H., Ruckenstuhl, C., Sigrist, C., Wissing, S., Kollroser, M., Frohlich, K.-U., Sigrist, S., and Madeo, F. (2007) *Cell* **25**, 233-246
23. Schafer, P., Scholz, S. R., Gimadutdinow, O., Cymerman, I. A., Bujnicki, J. M., Ruiz-Carrillo, A., Pingoud, A., and Meiss, G. (2004) *J. Mol. Biol.* **338**, 217-228
24. Hsia, K.-C., Li, C.-L., and Yuan, H. S. (2005) *Curr. Opin. Struct. Biol.* **15**, 126-134
25. Temme, C., Weissbach, R., Lilie, H., Wilsom, C., Meinhart, A., Meyer, S., Golbik, R., Schierhorn, A., and Wahle, E. (2009) *J. Biol. Chem.* **284**, 8337-8348
26. Loll, B., Gebhardt, M., Wahle, E., and Meinhart, A. (2009) *Nucleic acids research* **37**, 7312-7320
27. Brenner, S. (1974) *Genetics* **77**, 71-94
28. Mello, C. C., Krame, J. M., Stinchcomb, D., and Ambros, V. (1992) *EMBO J* **10**, 3959
29. Gu, T., Orita, S., and Han, M. (1998) *Mol Cell Biol* **18**, 4556-4564
30. Wang, X., Yang, C., Chai, J., Shi, Y., and Xue, D. (2002) *Science* **298**, 1587-1592
31. Miller, M. D., Cai, J., and Krause, K. L. (1999) *J. Mol. Biol.* **288**, 975-987
32. Moon, A. F., Midon, M., Meiss, G., Pingoud, A., London, R. E., and Pedersen, L. C. (2011) *Nucleic acids research* **39**, 2943-2953

33. Hsia, K.-C., Chak, K.-F., Liang, P.-H., Cheng, Y.-S., Ku, W.-Y., and Yuan, H. S. (2004) *Structure* **12**, 205-214
34. Hsu, D. R., and Meyer, B. J. (1994) *Genetics* **137**, 999-1018.
35. Galburt, E. A., Chevalier, B., Tang, W., Jurica, M. S., Flick, K. E., Raymond J. Monnat, J., and Stoddard, B. L. (1999) *Nature Struct. Biol.* **6**, 1096-1099
36. Sokolowska, M., Czapinska, H., and Bochtler, M. (2009) *Nucleic acids research* **37**, 3799-3810
37. Raaijmakers, H., Vix, O., Törõ, I., Golz, S., Kemper, B., and Suck, D. (1999) *EMBO J.* **18**, 1447-1458
38. Shen, B. W., Landthaler, M., Shub, D. A., and Stoddard, B. L. (2004) *J. Mol. Biol.* **342**, 43-56
39. Ghosh, M., Meiss, G., Pingoud, A., London, R. E., and Pedersen, L. C. (2005) *J. Biol. Chem.* **280**, 27990-27997
40. Li, C.-L., Hor, L.-I., Chang, Z.-F., Tsai, L.-C., Yang, W.-Z., and S.Yuan, H. (2003) *EMBO J.* **22**, 4014-4025
41. Luscombe, N. M., Laskowski, R. A., and Thornton, J. M. (2001) *Nucleic acids research* **29**, 2860-2874
42. Hsiao, Y.-Y., Yang, C.-C., L., L. C., Lin, J. L. J., Duh, Y., and Yuan, H. S. (2011) *Nature Chem. Biol.* **7**, 236-243
43. Flick, K. E., Jurica, M. S., Jr, R. J. M., and Stoddard, B. L. (1998) *Nature* **394**, 96-101
44. Biertümpfel, C., Yang, W., and Suck, D. (2007) *Nature* **449**, 616-620
45. Wu, S.-L., Li, C.-C., Chen, J.-C., Chen, Y.-J., Lin, C.-T., Ho, T.-Y., and Hsiang, C.-Y. (2009) *J. Biomed. Sci.* **16**, 6

Acknowledgments- Portions of this research were carried out at the National Synchrotron Radiation Research Center (BL-13B1 and BL-13C1), a national user facility supported by the National Science Council of Taiwan, ROC. The Synchrotron Radiation Protein Crystallography Facility is supported by the National Research Program for Genomic Medicine.

FOOTNOTES

* This work was supported by research grants from Academia Sinica (H.Y.), National Institute of Health GM79097 (D.X.), and the National Science Council, Taiwan, R.O.C. (H.Y.).

FIGURE LEGENDS

Figure 1. Sequence alignment of CPS-6/EndoG. Sequences of CPS-6/EndoG from *C. elegans, H. sapien, B. taurus, D. melanogaster and S. cerevisiae* are aligned and listed. CPS-6 shares a high sequence identity of 50%, 49%, 55% and 39% with human, bovine, fruit fly and yeast EndoG, respectively. The amino acid residues found in *H. sapien*, *B. taurus* and *D. melanogaster* important for metal ion coordination and DNA binding are colored in pink and brown, respectively (22,23,26,45). The ββα-metal finger motif (β4-β5-α4) is marked in orange, and the conserved ^{145}DRGH^{148} sequence is located in β4. The residues that are likely involved in DNA binding and that were subjected to site-directed mutagenesis in this study are colored in yellow. The secondary structures derived from the crystal structure of CPS-6 are depicted in green cylinders for α-helices and blue arrows for β-strands. MLS stands for mitochondrial localization sequence.

Figure 2. The recombinant CPS-6 is a functional homodimeric nuclease. (A) The purity of the recombinant CPS-6 (63-305) H148A mutant was assayed by 12% SDS-PAGE. (B) Size exclusion

chromatographic profile of CPS-6 H148A mutant showing that the protein was eluted at 74 ml, indicating a dimeric conformation. Protein markers used here are ferritin (440 kDa), catalase (232 kDa), bovine serum albumin (67 kDa), ovalbumin (44 kDa) and carbonic anhydrase (29 kDa). (C) Wild-type CPS-6 digests 1.6 kb linear DNA fragments (upper panel) in a concentration-dependent manner, whereas H148A has no nuclease activity (lower panel). Lane M is a DNA marker. (D) CPS-6 digests plasmid DNA most efficiently at pH 7. pET28 plasmid DNA (25 ng) was incubated for 1 h at 37°C with 2 μM CPS-6 in reaction buffer containing 25 mM NaCl, 2 mM $MgCl_2$, and 2 mM DTT with pH values ranging from 4 to 11. Lane M is a DNA marker, and lane C is a control in the absence of CPS-6. (E) CPS-6 digests plasmid DNA more efficiently at low salt concentrations (25 to 100 mM NaCl). (F) The immunoprecipitation experiment shows that the 6xHis-tagged CPS-6 (H148A mutant) interacts directly with the His-tagged WAH-1.

Figure 3. CPS-6 digests both DNA and RNA with a preference for G-track DNA. (A) CPS-6 digests pET28 plasmid DNA (25 ng) in a concentration-dependent manner (0.03 to 2 μM). Lane M is a DNA marker. (B) CPS-6 digests both 5'-end-^{32}P-labeled single-stranded DNA (48 nt) and double-stranded DNA (48 bp). (C) CPS-6 digests 11-mer ssRNA (5'-end-^{32}P-labeled 5'-AACCUUACAAC-3') and 11-mer ssDNA (5'-end-^{32}P-labeled 5'-AACCTTACAAC-3') substrate. All reactions (A-C) were carried out in the buffer of 10 mM HEPES, pH 7.0, 100 mM NaCl, 2 mM $MgCl_2$, and 2 mM DTT for 1 h at 37°C. Lanes C are controls in the absence of CPS-6. (D) The binding constants between CPS-6 H148A mutant and the 14-nt 5'-end-^{32}P-labeled ssDNA containing different lengths of poly(dG) were measured by nitrocellulose filter binding assays. The dissociation constants between CPS-6 H148A and ssDNA containing 0 (open triangle), 2 (circle), 4 (triangle) and 6 G (closed rectangle) are 5.14±0.36 μM, 2.54±0.21 μM, 1.13±0.73 μM and 0.53±0.02 μM, respectively. Error bars are generated from three independent experiments.

Figure 4. Crystal structure of the Mg^{2+}-bound CPS-6 H148A mutant. (A) Side view of the overall crystal structure of the dimeric CPS-6 (residues 63-305, H148A mutant) that was determined at 1.8 Å resolution (PDB code: 3S5B). The two protomers are displayed in pink and grey, respectively. The ββα-metal finger motifs are displayed in cyan with a Mg^{2+} ion (orange sphere) bound at the active site. (B) Omit map illustration for the active site of CPS-6 with the Mg^{2+} and the coordinated water molecules omitted for the map calculation (contoured at 3.0σ). (C) Top view of the molecular model of CPS-6 bound with DNA. This model was constructed by superimposition of the ββα-metal finger motif in CPS-6 (residues 144-155 and 170-182) with that of the Vvn-DNA complex (PDB code: 1OUP) to determine where the DNA (GCGATCGC) is bound on CPS-6. A positively-charged surface (in blue) near the active site of CPS-6 interacts well with the DNA phosphate backbone. The Mg^{2+} ion in the active site is displayed as a green ball.

Figure 5. Identification of the residues involved in DNA binding in CPS-6. (A) Side view of a model of CPS-6 homodimer bound with two DNA molecules. The ββα-metal motif is colored in cyan and the Mg^{2+} ion in orange. The dsDNA molecules are colored in yellow. (B) The top view of CPS-6-DNA complex model suggests that several basic and aromatic amino acid residues (in blue) are located closely to the DNA backbones, likely involved in protein-DNA interactions, including R117, F122, R146, R156 and F166. (C) The DNA digestion assays show that a mutation at F122, R146, R156 and F166, but not at R117, greatly reduced the DNase activity of CPS-6, suggesting that these residues are involved in DNA binding and/or digestion. The integrated density values (in %, as normalized using the control DNA as 100 %) for the undigested full length 5'-end-^{32}P-labeled ssDNA

used in this study are summarized as a histogram. (E) The dissociation constants between CPS-6 mutants and DNA (5'-end-^{32}P-labeled 48-nt ssDNA) were measured by filter binding assays. The dissociation constants are shown in the histogram: 245±18 nM for H148A, 249±20 nM for H148A/R117A, 707±88 nM for H148A/F122A, 468±42 for H148A/R146A, 652±111 nM for H148A/R156A and 658±74 nM for H148A/F166A.

Figure 6. The cell death assay in *C. elegans*. Transgenic *cps-6(sm116)* animals expressing wild-type CPS-6 (A), CPS-6(H148A) (B), CPS-6(R146A) (C), or CPS-6(F166A) (D) under the control of the *dpy-30* promoter were generated and the number of cell corpses were scored. For each construct, data were collected from three independent transgenic lines. Stages of transgenic embryos examined were: comma, 1.5-fold, 2-fold, 2.5-fold, 3-fold and 4-fold. The y-axis represents the average number of cell corpses scored and error bars are standard deviations. Fifteen embryos were counted for each developmental stage. The significance of differences were determined by two-way ANOVA, followed by Bonferroni comparison. *, $P < 0.001$; **, $P < 0.05$. All other points had P values > 0.05.

Figure 7. The active site and proposed catalytic mechanism for CPS-6. (A) The active site of CPS-6 shares a similar conformational arrangement with that of Vvn. The ββα-metal finger motif is colored in cyan, with the conserved ^{145}DRGH^{148} sequence (and the corresponding ^{77}EWEH^{80} sequence in Vvn) displayed in marine blue. (B) Schematic diagram of the proposed DNA hydrolysis mechanism by CPS-6. H148 acts as a general base to activate a water molecule which in turn makes an in-line attack on the scissile phosphate. The magnesium ion stabilizes the phosphoanion transition state and the Mg^{2+}-bound water molecule functions as a general acid to provide a proton to the 3'-oxygen leaving group.

Figure 8. Structural comparison of non-specific and site-specific dimeric ββα-metal finger nucleases. (A) The overall folds of the two non-specific nucleases, CPS-6 and *Serratia* nuclease, are similar. However, the dimeric interfaces are located in different regions as revealed by the superimposition of one protomer of the two proteins (boxed in the right panel). (B) The crystal structures of the three site-specific endonucleases Hpy99I, I-PpoI and T4 Endo VII in complex with their DNA substrates show that the two ββα-metal motifs are positioned and oriented next to the DNA sugar-phosphate backbones. The 2-fold symmetry (displayed as an oval) of the dimeric proteins coincides roughly with the 2-fold axis of the DNA substrates.

Table 1. Crystallographic statistics of CPS-6

Data collection and processing	
Wavelength (Å)	1.0
Space group	$P2_1$
Cell dimensions (a, b, c/ β) (Å/ degree)	69.2, 45.4, 80.3/ 104.2
Resolution (Å)	1.8-37.6 (1.80-1.83)*
Observed/unique reflections	130,358/44,074
Data redundancy	3.0 (2.9)
Completeness (%)	95.9 (100)
R_{sym} (%)	8.5 (34.8)
$I/\sigma(I)$	20.1 (4.7)
Refinement statistics	
Resolution range	1.8-37.6
Reflections (work/test)	41,201/1,876
R-factor/R-free (%)	16.6/21.0
Number of non-hydrogen atoms-	
Protein/metal ions/water molecules	3,836/2/430
Model quality	
RMSD in bond length (Å)/bond angle (^{o})	0.007/1.043
Average B-factor-	
protein/metal/solvent (Å^2)	12.6/14.1/25.5
Ramachandran plot-	
Most favored	98
Additionally allowed	0.5
Generally allowed	1.5
Disallowed	0

*Values in parentheses refer to the highest resolution shell.

Figure 1

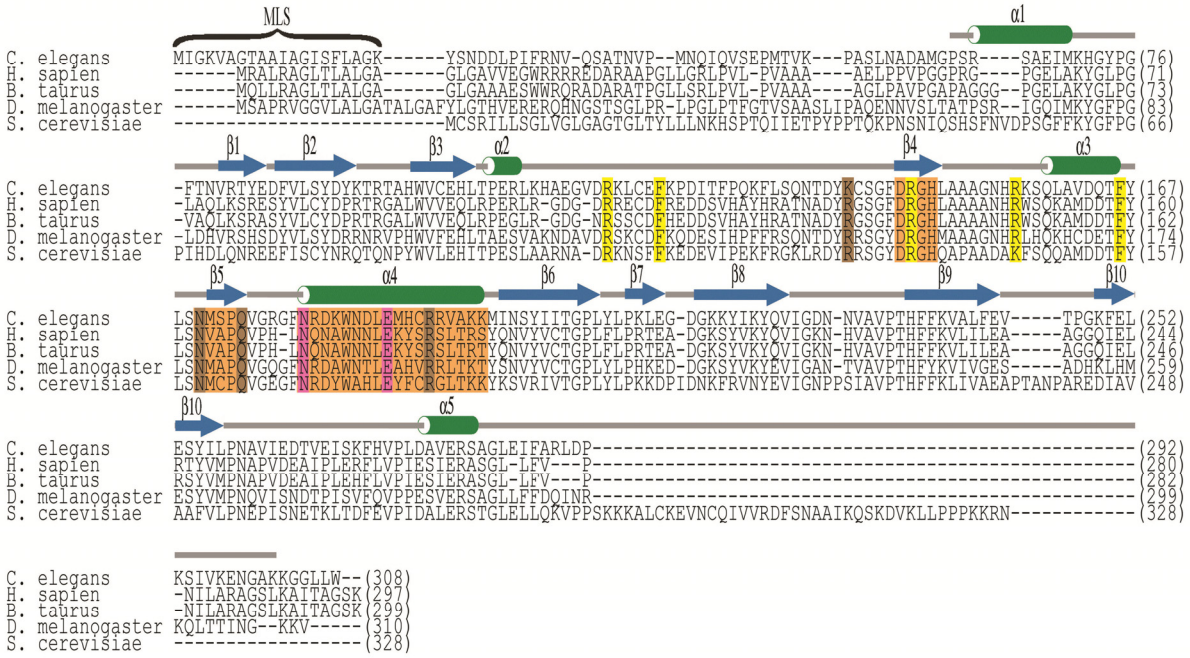

Figure 2

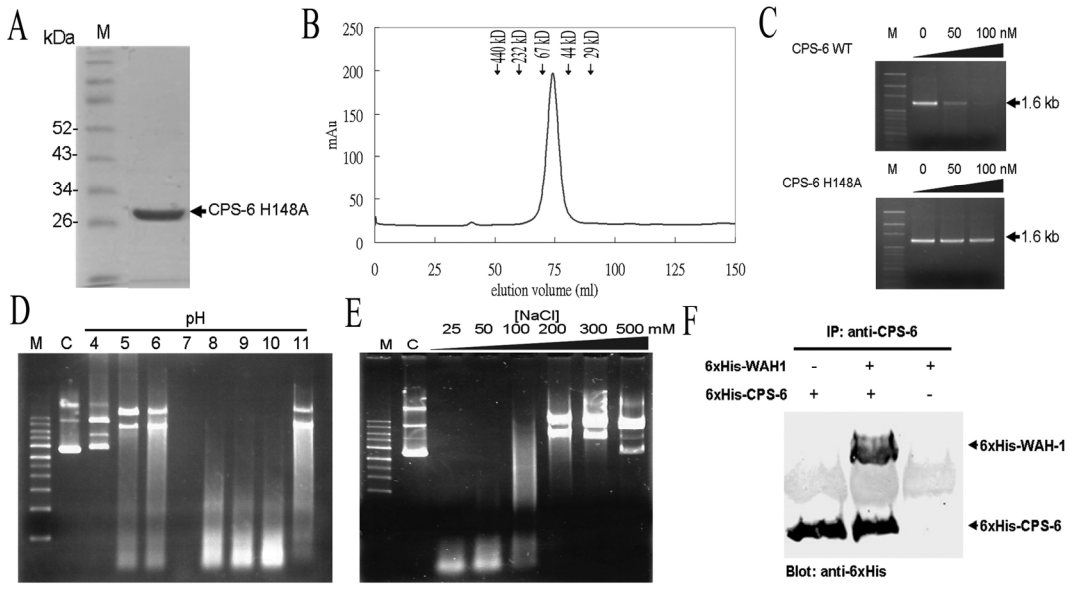

Figure 3

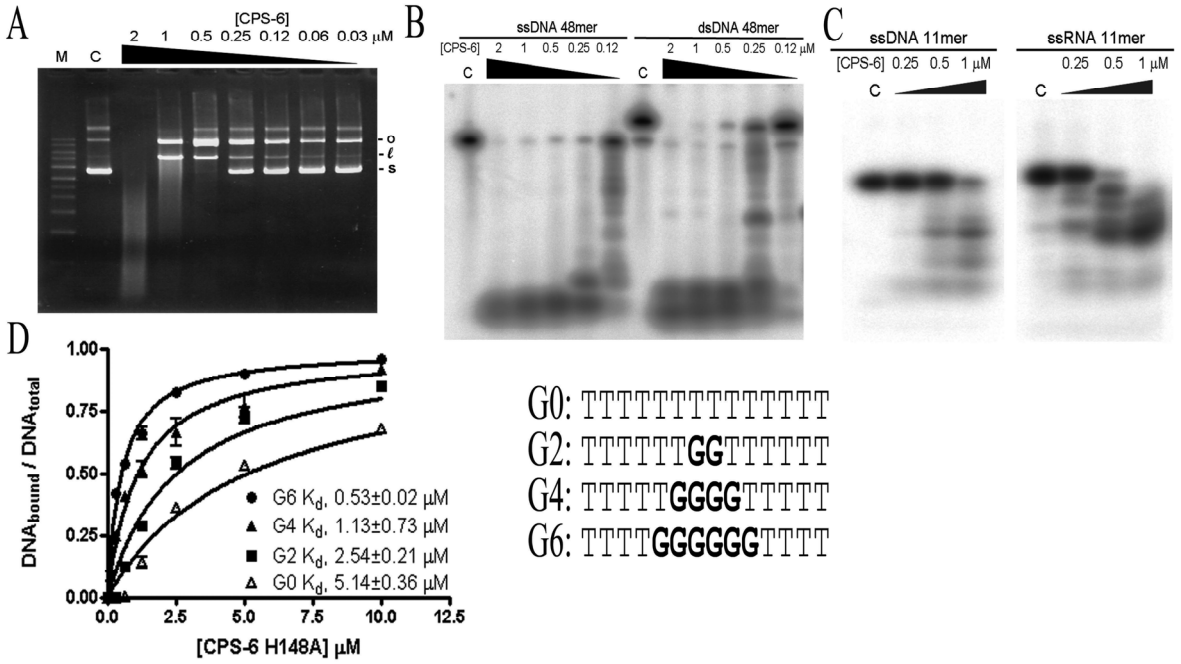

Figure 4

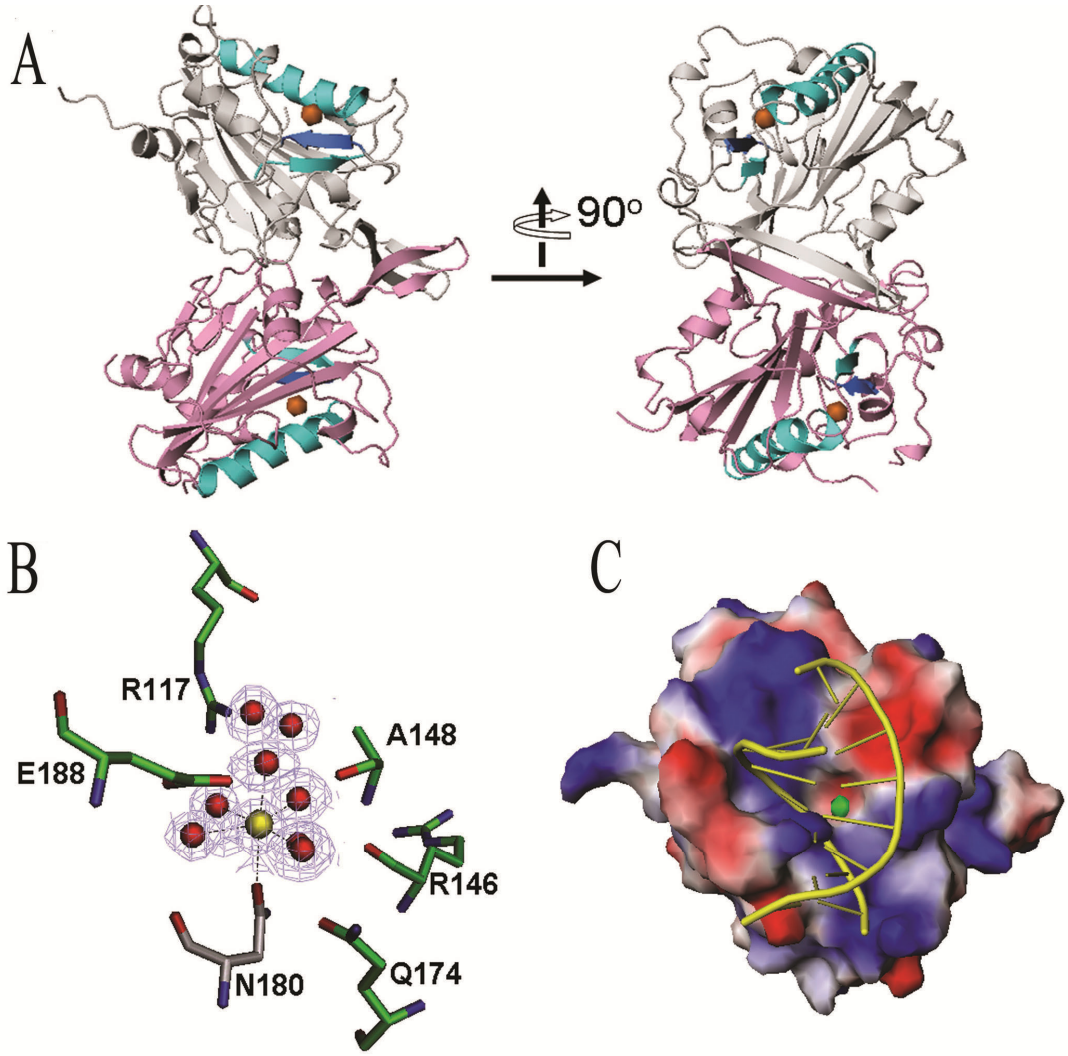

Figure 5

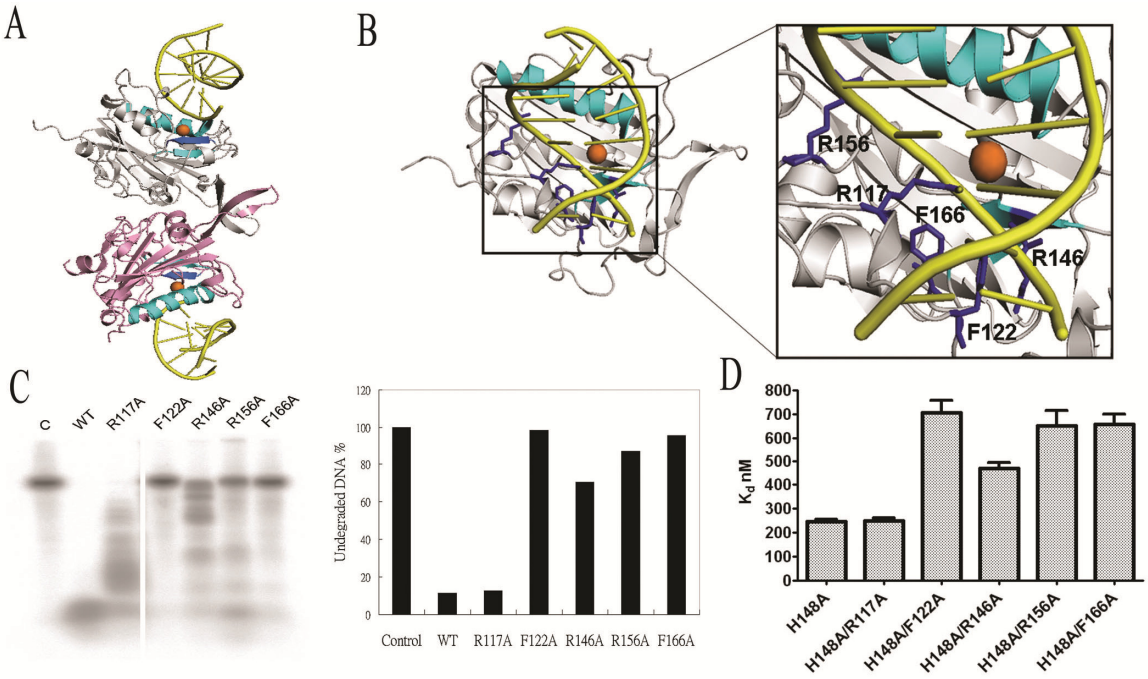

Figure 6

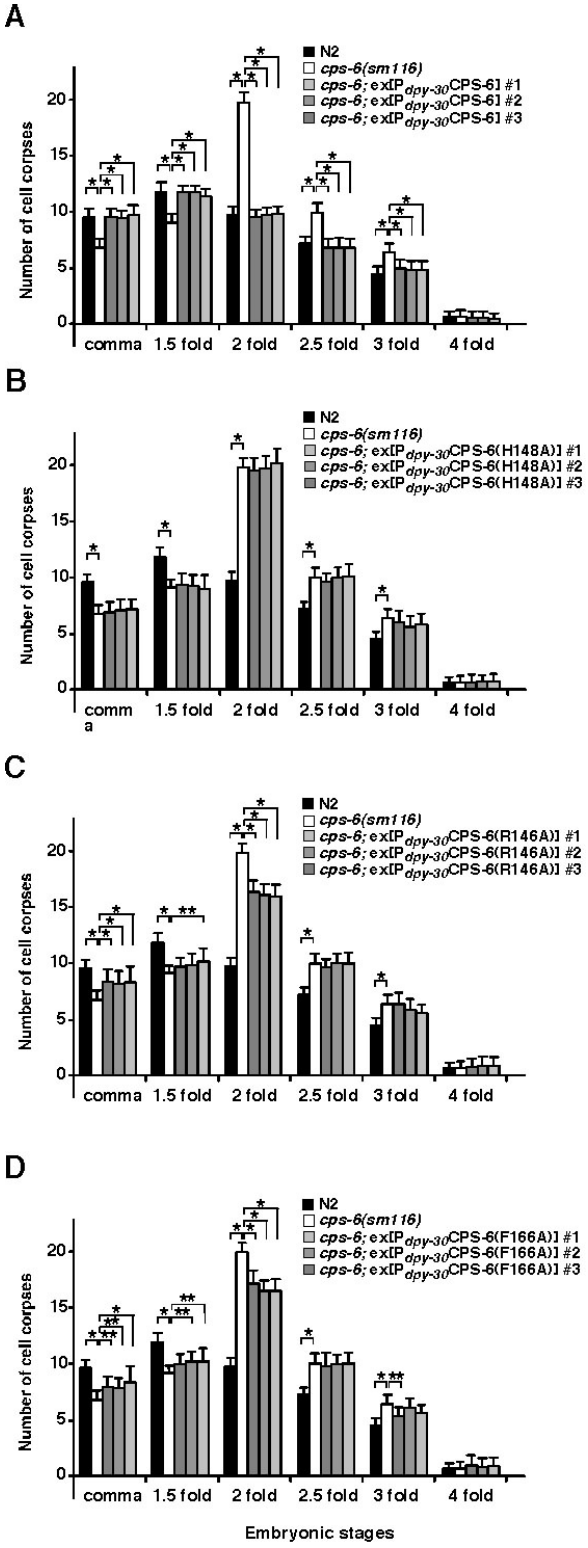

Figure 7

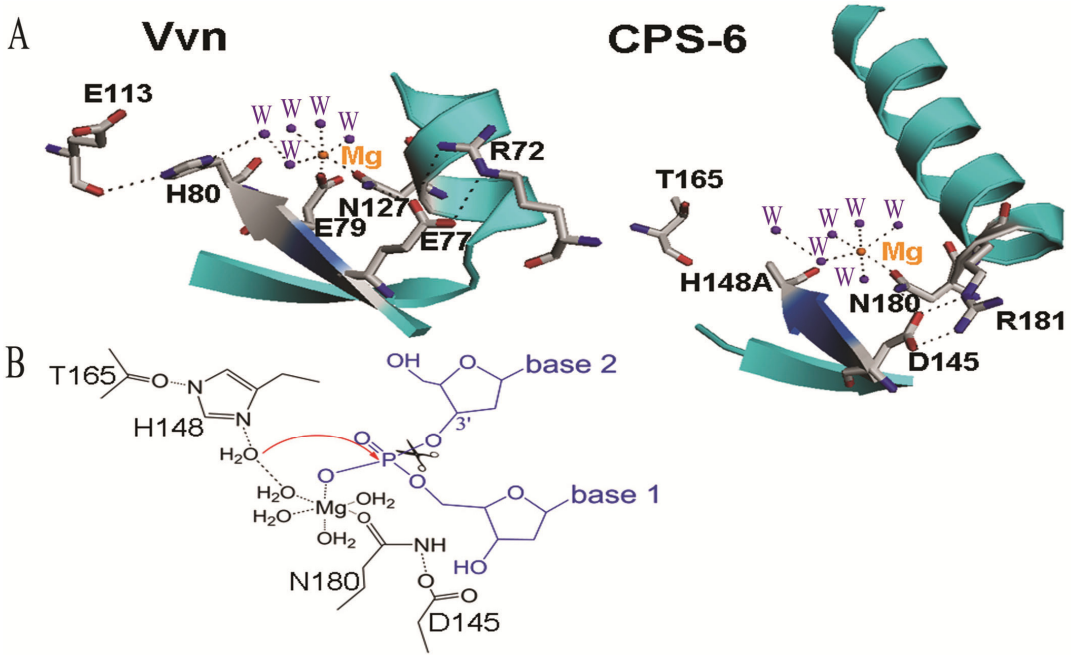

Figure 8

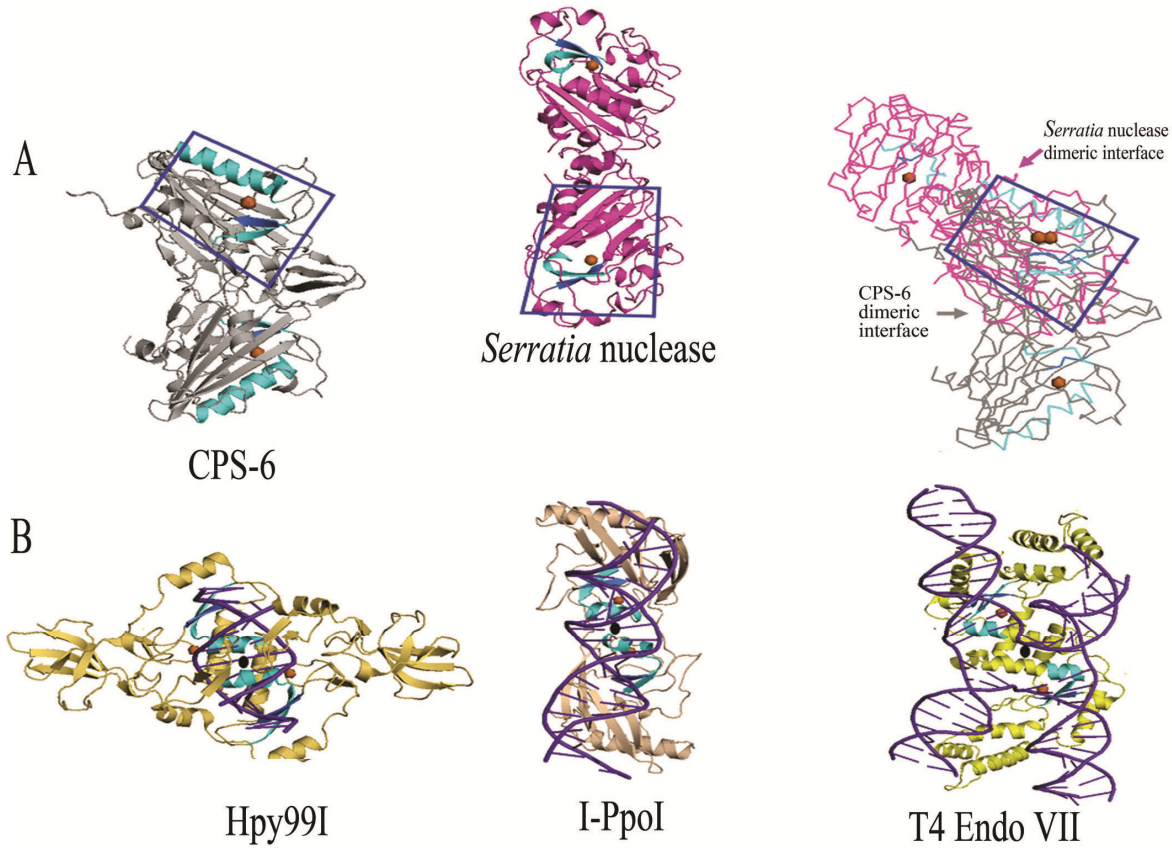

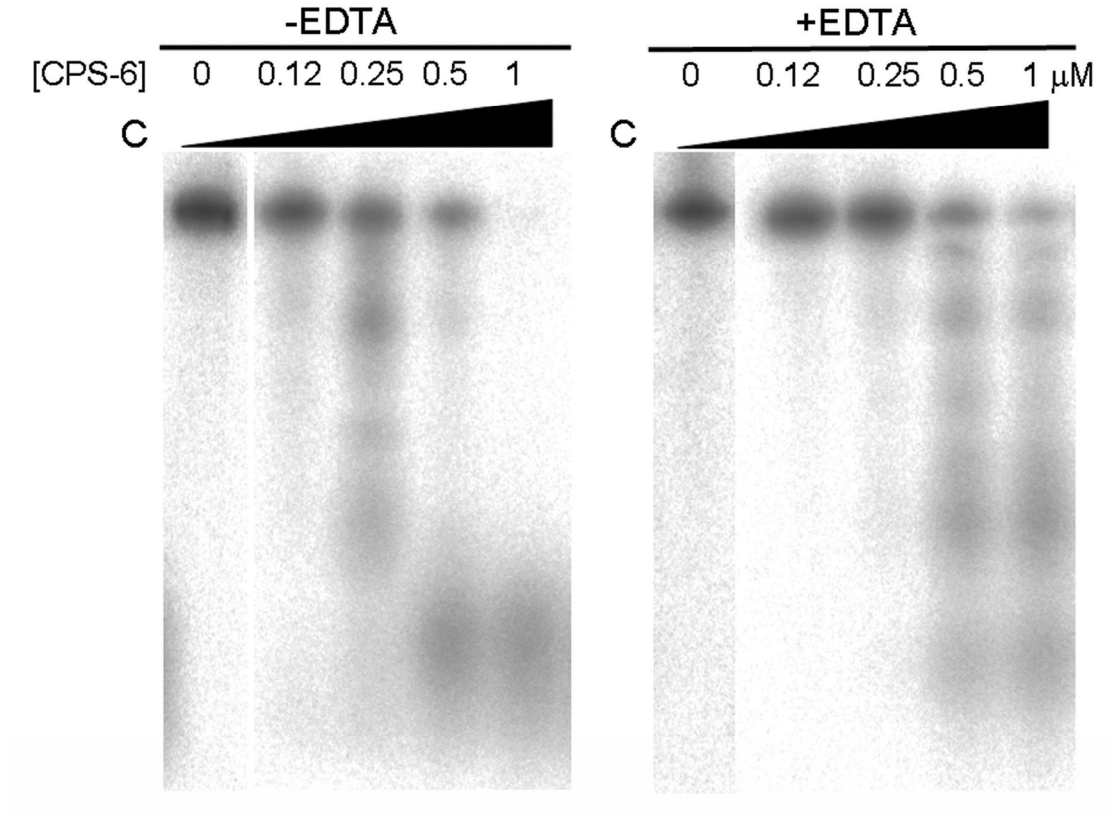

Supplemental Figure S1. Divalent metal ions are required for CPS-6 nuclease activity. The 5'-end-^{32}P-labeled single-stranded DNA (48 nt) were incubated with CPS-6 (0 to 1 μM) in the absence and presence of 2 mM EDTA in 10 mM HEPES (pH 7.0), 100 mM NaCl and 2 mM DTT. The digested DNA samples were resolved in a 20% denaturing polyacrylamide gel (8 M urea). The DNase activity of CPS-6 reduced significantly in the presence of EDTA.

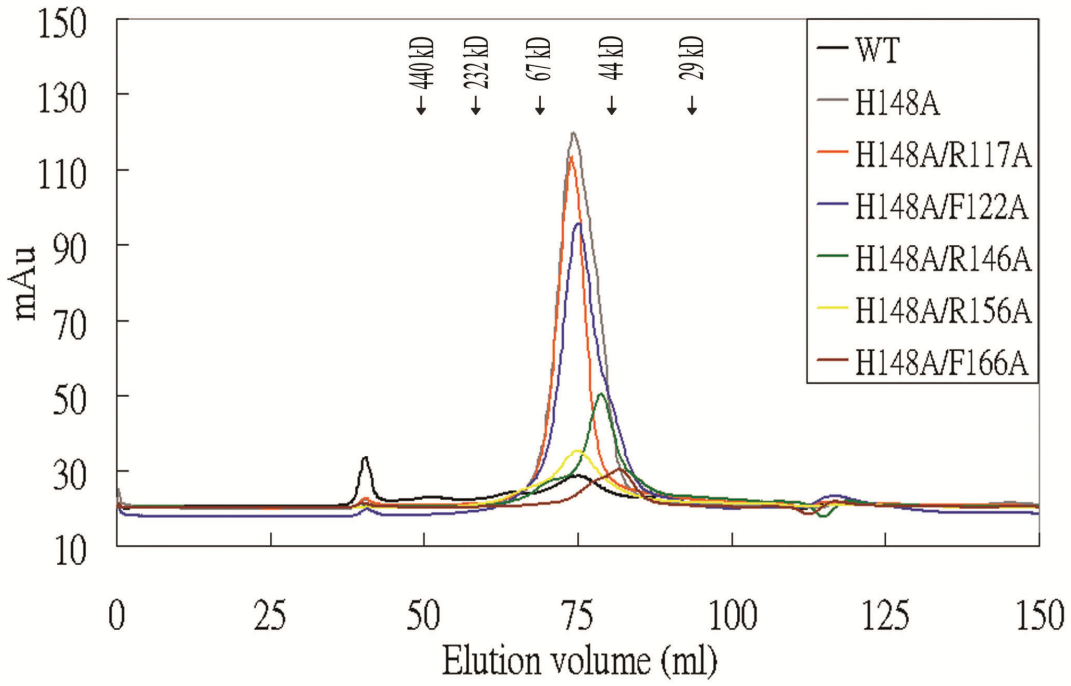

Supplemental Figure S2. Size exclusion chromatographic profiles for CPS-6 wild-type and mutant proteins. All the proteins were eluted at 74-81 ml, indicating a dimeric conformation. Protein markers: ferritin (440 kDa), catalase (232 kDa), bovine serum albumin (67 kDa), ovalbumin (44 kDa) and carbonic anhydrase (29 kDa) (see EXPERIMENTAL PROCEDURES).